JBIC Journal of Biological Inorganic Chemistry (2018) 23:1105–1118
https://doi.org/10.1007/s00775-018-1607-z

ORIGINAL PAPER

Mercury-induced aggregation of human lens γ-crystallins reveals a potential role in cataract disease

J. A. Domínguez-Calva[1] · M. L. Pérez-Vázquez[1] · E. Serebryany[2] · J. A. King[2] · L. Quintanar[1]

Received: 30 June 2018 / Accepted: 22 August 2018 / Published online: 30 August 2018

Abstract

Cataract disease results from non-amyloid aggregation of eye lens proteins and is the leading cause of blindness in the world. A variety of studies have implicated both essential and xenobiotic metals as potential etiological agents in cataract disease. Essential metal ions, such as copper and zinc, are known to induce the aggregation in vitro of human γD crystallin, one of the more abundant γ-crystallins in the core of the lens. In this study, we expand the investigation of metal–crystallin interactions to heavy metal ions, such as divalent lead, cadmium and mercury. The impact of these metal ions in the non-amyloid aggregation, protein folding and thermal stability of three homologous human lens γ-crystallins has been evaluated using turbidity assays, electron microscopy, electronic absorption and circular dichroism spectroscopies. Our results show that Hg(II) ions can induce the non-amyloid aggregation of human γC and γS crystallins, but not γD crystallin. The mechanism of Hg-induced aggregation involves direct metal–protein interactions, loss of thermal stability, partial unfolding of the N-terminal domain of these proteins, and formation of disulfide-bridged dimers. Putative Hg(II) binding sites in γ-crystallins involved in metal-induced aggregation are discussed. This study reveals that mercury ions can induce the aggregation of human lens proteins, uncovering a potential role of this heavy metal ion in the bioinorganic chemistry of cataract disease.

Electronic supplementary material The online version of this article (https://doi.org/10.1007/s00775-018-1607-z) contains supplementary material, which is available to authorized users.

Extended author information available on the last page of the article

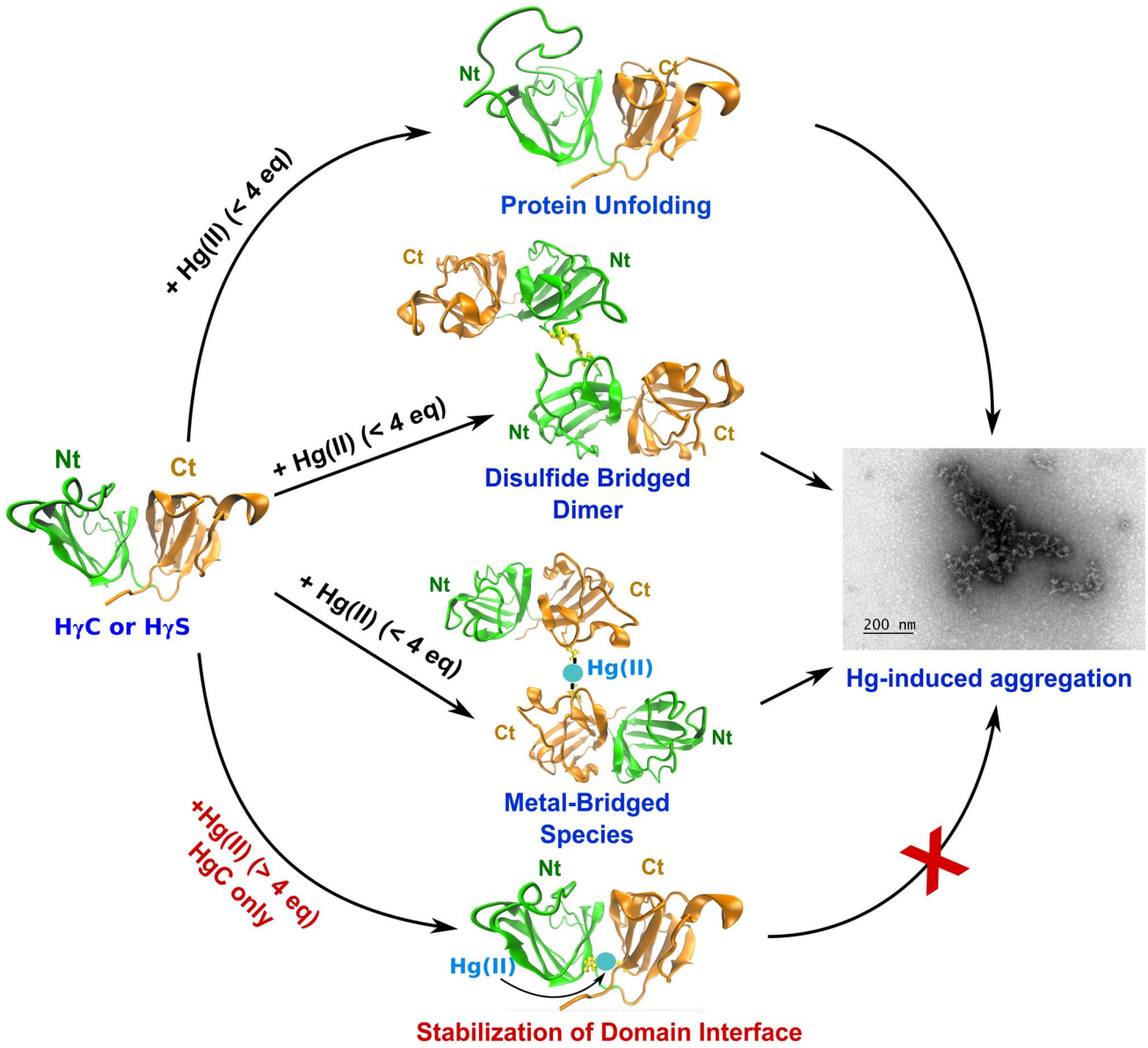

Keywords Lens crystallins · Human gamma crystallin · Mercury · Heavy metal ions · Cataract disease

Introduction

Cataract disease is the number one cause of blindness in the world, affecting over 60 million people worldwide [1]. Cataracts are formed upon aggregation of lens proteins into light-scattering high molecular weight complexes that cause lens opacity. Human lens transparency depends on the solubility and stability of crystallins, the most abundant proteins in the lens [2, 3]. The only available treatment for cataract is eye surgery, which is costly and it is not risk free. Developed countries like the USA spend billions of dollars per year in cataract surgery, while in developing countries cataract has become the major cause of visual disability [4].

Congenital cataracts are due to mutations in the genes that code for lens crystallin proteins [5], while sporadic cataract disease is caused by damage to these proteins throughout the lifetime, including oxidation, deamidation, glycation, racemization and truncation [2, 6–9]. Covalent modifications of crystallins can lead to the formation of partially folded intermediates that are prone to non-amyloid aggregation [2, 3]. Crystallins are classified as: α-crystallins, which are of small heat shock proteins; the dimeric and oligomeric

β-crystallins, and the monomeric γ-crystallins [3, 10, 11]. α-crystallins are able to recognize partially folded damaged β- and γ-crystallins, binding them to prevent their aggregation [2, 12]. The lens is formed of elongated fiber cells with high protein content, depleted of nuclei and organelles; this unique cell differentiation occurs in the embryonic stage [13]. Fully differentiated fiber cells have a very low metabolism, and are unable to synthesize new proteins, nor to degrade damaged lens proteins. Thus, in an aged lens, when the chaperone α-crystallins are depleted, further damage to lens crystallins cause development of cataract. Indeed, cataract incidence is strongly associated with aging.

Native γ-crystallins are highly soluble and stable, but in vitro chemical or thermal denaturation have shown to lead to the formation of partially folded intermediates that are prone to aggregation [2, 3]. The N-terminal domain has shown to be less stable, as compared to the C-terminal domain [14]. Studies of mutations associated with congenital cataract have also shed light on the mechanisms of the non-amyloid aggregation of γ-crystallins [15–19]. Overall, a domain swapping mechanism has been proposed, involving interactions between partially destabilized crystallins [2]. Interestingly, a recent structural study has identified the conservation of a native-like fold in non-amyloid aggregates of a cataract-associated mutation in human γD crystallin [20]. Thus, small perturbations in the protein fold and stability of γ-crystallins may be enough to cause non-amyloid aggregation, while a native-like fold is preserved.

A variety of studies have implicated metals as a potential etiological agent in cataract disease. Cataract is well documented among workers in metal-working industries [21]. The concentration of metal ions, such as copper and zinc, in cataractous lenses are increased significantly, as compared to normal lenses, suggesting a potential role of these essential metals in cataract disease [22–24]. Indeed, metal ion levels in the human lens change upon normal aging and can also be influenced by habits, such as smoking [24, 25]. Smoking is a major risk factor for cataract disease [26, 27] and it is well documented as a major source of metals, such as cadmium and lead [28]. Accumulation of copper, lead and cadmium has been identified in cataractous lenses from cigarette smokers [24, 25]. On the other hand, environmental exposure and elevated blood levels of mercury have been associated with an increased risk for age-related cataract disease [29]. These observations suggest a potential role of heavy metal ions in cataract disease pathology. Environmental exposure to heavy metal ions—e.g., from airborne particles from glass manufacturing [30]—is indeed a public concern, as xenobiotic metals such as lead, cadmium and mercury can hijack the trafficking mechanisms in place for essential metal ions in the human body, accumulating in several tissues and causing a variety of toxic effects through oxidative mechanisms [31].

The interaction of metal ions with lens crystallin proteins has been relatively unexplored. Essential metal ions such as Cu(II) and Zn(II) are known to bind to the chaperone α-crystallins [32–35], while they can also induce the non-amyloid aggregation of human γD crystallin (HγD), one of the more abundant γ-crystallins in the core of the lens [36]. In particular, the mechanism of copper-induced aggregation of HγD crystallin involves loss of protein stability and formation of partially folded intermediates that lead to high molecular weight light-scattering aggregates. Metal-induced aggregation of HγD crystallin involves site-specific interactions with the protein, revealing a novel bioinorganic facet of cataract disease. In this study, we expand these investigations to evaluate the impact of heavy metal ions in the stability and aggregation of γ-crystallins.

The monomeric γ-crystallins are structural lens proteins that contain four Greek key motifs organized into two domains [3]. The mammalian genome contains seven γ-crystallin genes; the γ-A-F-crystallin genes are most copiously expressed in early lens development, thus their products are mainly found in the lens core region, while γS crystallin is expressed solely in the cortical region of the lens [5]. The human γD-, γS-(HγS), and γC-(HγC) crystallins are among the most abundant structural proteins in the human lens, comprising 11%, 9% and 7%, respectively, of the total protein content in young human eye lenses [37]. In this study, we use these three γ-crystallin proteins as a case study to explore the effects of heavy metal ions, such as Pb(II), Hg(II) and Cd(II), in protein stability and aggregation, events that could be associated with the mechanisms of toxicity of heavy metal ions and particularly with the potential role of these metals in the development of cataract disease.

Materials and methods

Plasmids and site-directed mutagenesis

Plasmids encoding tagless HγC, HγD and HγS crystallins were used. For HγC and HγD crystallins, pET16b plasmids lacking the His tag were used, as previously described [38–41]. For HγS crystallin, the coding sequence was amplified from a pQE1-HγS plasmid [42], flanked by NcoI and XhoI restriction enzyme sites. The HγS insert was ligated into a pET15b NcoI/XhoI plasmid, using a Gibson Assembly kit (New England Biolabs), yielding a tagless HγS contruct. For HαB crystallin a pAED4 plasmid was used, as previously described [43].

Site-directed mutagenesis of γ-crystallins was performed using a Q5 site-directed mutagenesis kit from BioLabs. Table S1 lists the oligonucleotide primers used for each mutation. The DNA plasmids obtained after mutagenesis

were sequenced with the T7 promoter primer and were found to contain the desired mutation, but no other sequence changes.

Recombinant human γ-crystallin expression and purification

Recombinant HγC, HγD, and HγS crystallins were expressed in BL21-RIL *E. Coli*, and purified by ammonium sulfate precipitation followed by size exclusion chromatography (SEC), as previously described [36, 38–41]. Briefly, this involves growing cells at 37 °C in super broth to an optical density of ~ 5 at 600 nm. Protein expression was induced with 1 mM isopropyl β-D-1-thiogalactopyranoside (ITPG) at 18 °C overnight. Harvested cells from a 2 L culture growth were resuspended with 10 mM ammonium acetate buffer, pH 7, 50 mM NaCl, to a total volume of 50 mL. Cells were lysed by incubation with lysozyme (1 mg/mL) and DNase (20 ng/mL) for 30 min, in the presence of EDTA-free Complete Mini Protease Inhibitor Cocktail (Roche), followed by 10–15 sonication cycles (30 s each) in ice. Lysate was centrifuged at 17,000*g* for 45 min, and ammonium sulfate was slowly added to the supernatant to reach 30% (w/v), while stirring in ice. The proteins that precipitated at 30% ammonium sulfate were discarded, and more ammonium sulfate was added to reach 50% (w/v) and cause γ-crystallin precipitation. The precipitate was resuspended in 10 mM ammonium acetate buffer, pH 7, with 50 mM NaCl, spun down, and passed through a 0.2 μm filter before loading into an SEC column (Hi-Prep Sephacryl S-100), using a fast protein liquid chromatography (FPLC) instrument (GE Life Sciences). Eluted γ-crystallin fractions were analyzed by SDS-PAGE to verify purity, pooled and stored at 4 °C. Protein concentration was determined by electronic absorption spectroscopy, using the extinction coefficient $\varepsilon = 41\ cm^{-1}mM^{-1}$ for all γ-crystallins.

Turbidity assays

Crystallin proteins (50 μM) were incubated in 10 mM ammonium acetate buffer, pH 7.0, with 50 mM NaCl, in the absence or presence of metal ions, at 37 °C (unless otherwise stated), in a total volume of 200 μL. Metal ions were added to the buffer solutions and pre-equilibrated at 37 °C before addition of the protein. Samples were incubated and analyzed in a FluoStar Optima 96-well plate reader. Absorbance at 400 nm was monitored every 60 s, shaking 10 s before each measurement. $CdCl_2$, $Pb(NO_3)_2$ and $HgCl_2$ salts were used as source of Cd(II), Pb(II) and Hg(II) ions; however, it should be noted that no effect of the counterion was observed, as mercury or cadmium acetate and lead chloride salt yielded identical results. No turbidity was detected in the control experiments with protein in the sample buffer, or for sample buffer with ten equiv of metal ions in the absence of protein. For each experiment, kinetic traces were baseline corrected using the control trace of sample buffer only. Turbidity assays were run at least four times for each condition.

Transmission electron microscopy

Protein aggregates from the end point of turbidity assays were diluted twofold with water, incubated onto glow-discharged carbon-coated Cu-Formvar grids (Ted Pella) for 1 min, blotted with filter paper, stained with uranyl acetate (1.5% w/v) for 30 s and dried. Grids were imaged in a Jeol-1400 EX transmission electron microscope.

CD spectroscopy

γ-Crystallins were characterized by circular dichroism, in the absence and presence of Hg, Cd or Pb ions. Independent solutions of 2 μM protein in 5 mM potassium phosphate buffer, pH 7.0, with 5 mM NaCl with the indicated amount of metal ion were prepared. CD spectra were collected in a Jasco J-815 CD spectropolarimeter.

UV–visible absorption spectroscopy

Room temperarure absorption titrations were recorded using an Agilent 8453 diode array spectrometer at room temperature. A 1 cm path length quartz cell was used, and spectra were recorded between 200 and 400 nm sampling points. Independent solutions of 5 μM protein in 5 mM potassium phosphate buffer, pH 7.0, with 5 mM NaCl with the indicated amount of metal ion were prepared.

Results and discussion

Hg(II) ions specifically induce the aggregation of HγC and HγS crystallins, but not HγD crystallin

The effect of adding 0–10 equiv of Pb(II), Cd(II) or Hg(II) ions to a 50 μM solution of H**γ**D, H**γ**C or H**γ**S crystallin was evaluated by turbidity assays (Figure S1). In these assays, an increase in turbidity reports the formation of large light-scattering protein aggregates. While Pb(II) and Cd(II) had very small effects in the aggregation of these proteins, Hg(II) ions specifically induced significant aggregation of HγC and HγS crystallins, but not H**γ**D crystallin at the protein concentration used (Fig. 1a–c). It should be noted that the effect

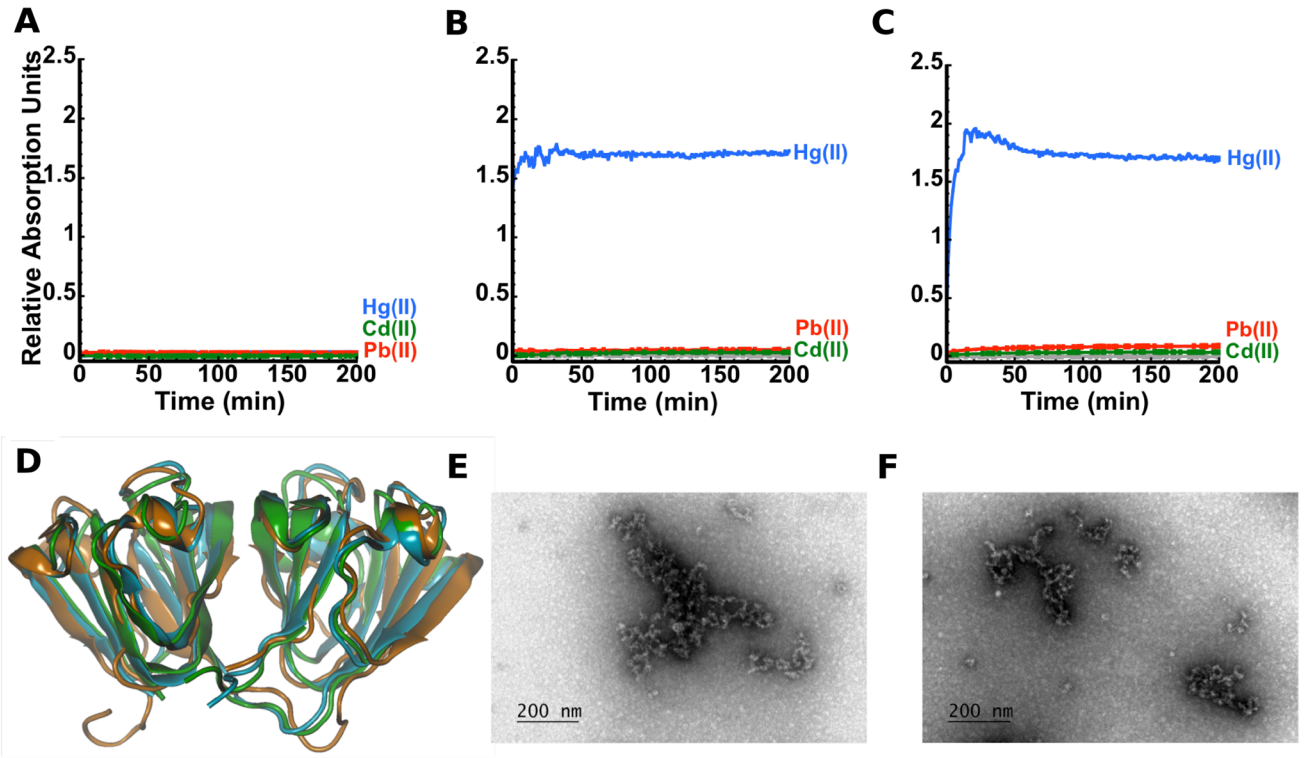

Fig. 1 Turbidity assays of HγD (**a**), HγC (**b**), HγS (**c**) crystallins (50 μM) in the absence (gray trace) or presence of 6 equiv of Pb(II) (red trace), Cd(II) (green trace) or Hg(II) (blue trace). All assays were performed at 37 °C, and turbidity at 400 nm was followed after the addition of metal ion. A structure alignment of HγD (light blue), HγC (green) and HγS (orange) crystallins is shown in (**d**). Electron microscopy images for Hg-induced aggregates of HγC (**e**) and HγS (**f**) crystallins, at the end point of the turbidity assays with 4 equiv of Hg(II)

of the Hg(II) ions is independent on the counter anion used (Figure S2). Although these γ-crystallins are homologous and have a double Greek key fold with high β-sheet content (Fig. 1d), it is very interesting to note that H**γ**D crystallin is not susceptible to Hg-induced aggregation, in spite of its homology with the other two γ-crystallins. The nature of the Hg-induced aggregates is non-amyloid, as probed by electron microscopy (Fig. 1e, f). Turbidity assays reveal that the extent of Hg-induced aggregation of H**γ**C and H**γ**S crystallins highly depend on the metal:protein ratio, but with distinct features for each protein (Fig. 2). For H**γ**S crystallin, the extent of aggregation increases steadily with the number of equivalents of Hg(II) added and saturates at four equiv (Fig. 2b and blue trace in Fig. 2h). This behavior indicates that there is a metal-dependent event that initiates mercury-induced aggregation of H**γ**S crystallin, and it saturates at four equiv of metal ion. In contrast, Hg-induced aggregation of H**γ**C crystallin reaches a maximum at three equiv of metal ion and then significantly decreases at higher metal:protein ratios (Fig. 2a and blue trace in Fig. 1g), revealing that different competing mechanisms may be at work, with opposing effects on the mercury-induced aggregation of H**γ**C crystallin.

Hg(II) ions induce loss of thermal stability and secondary structure of HγC and HγS crystallins

Thermal denaturation experiments on H**γ**C and H**γ**S crystallins were performed to assess the impact of Hg(II) ions in the thermal stability of these proteins. This was assessed by circular dichroism (CD) spectroscopy, monitoring the intensity of the negative signal at 218 nm that is indicative of β-sheet secondary structure, as a function of the temperature of the protein sample. H**γ**C and H**γ**S crystallins are stable proteins that can be heated up to 70 °C with no apparent effect on their secondary structure. However, at higher temperatures the CD signal at 218 nm decreases significantly, indicating thermal denaturation. Figure 2c, d shows the thermal denaturation curves for H**γ**C and H**γ**S crystallin, respectively, expressing the fraction of the protein that has unfolded as a function of temperature. The midpoint of each curve corresponds to the temperature at which approximately half of the protein retains its native conformation (T_m). For H**γ**S crystallin, a $T_m = 76.78 \pm 0.16$ °C can be determined (Fig. 2d and Table S2), consistent with previous reports [44]. However, when the thermal denaturation experiment is performed in the presence of 1–10 equiv of Hg(II) ions, the value of the

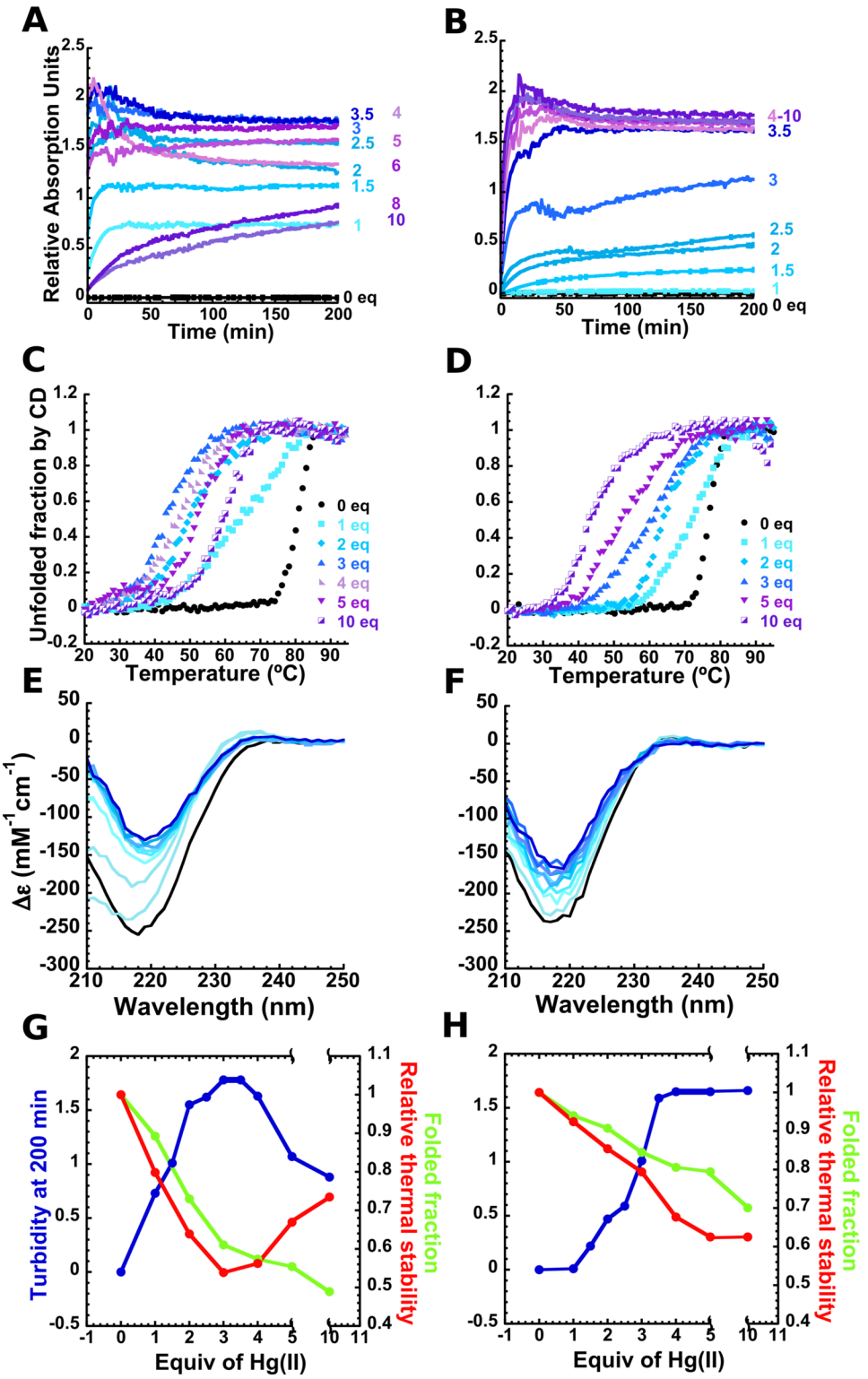

Fig. 2 Turbidity assays of HγC (**a**) and HγS (**b**) crystallins (50 μM) in the absence (dark trace) or presence of 1, 1.5, 2, 2.5, 3, 3.5 (light to dark blue), 4, 5, 6, 8 and 10 equiv of Hg(II) (light to dark purple traces). All assays were performed at 37 °C, and turbidity at 400 nm was followed after the addition of Hg(II). Thermal denaturation of HγC (**c**) and HγS (**d**) crystallins (2 μM) was followed by CD in the presence of 0, 1, 2, 3, 4, 5 or 10 equiv of Hg(II). The fraction of unfolded protein is plotted as a function of temperature, and the associated T_m values are listed in Table S2. Titrations of HγC (**e**) and HγS (**f**) crystallins (2 μM) with 0 (black spectra), 1, 2, 3, 4, 5, 6, 7, 8, 9 and 10 equiv of Hg(II) (light to dark traces), as followed by CD at 20 °C. Traces for turbidity, fraction of folded protein and relative thermal stability, as a function of the number of equivalents of Hg(II) ions for HγC (**g**) and HγS (**h**) crystallins are also plotted

T_m significantly decreases (down to 48.01 ± 0.02 °C for 10 equiv), while the shape of the curve is also affected (Fig. 2d and Table S2). The impact of Hg(II) ions in the thermal stability of HγS crystallin is directly proportional to the metal:protein ratio, as shown in the red trace in Fig. 2h, while it is inversely proportional to the extent of aggregation observed at the end point of the turbidity assay at each metal concentration (blue trace in Fig. 2h).

In contrast, thermal denaturation experiments of HγC crystallin in the presence of 1–10 equiv of Hg(II) ions

display a distinct behavior (Fig. 2c and Table S2). A $T_m = 80.38 \pm 0.05$ °C can be determined for HγC crystallin in the absence of metal ions. However, while the first 3 equiv of Hg(II) induce a drastic loss of thermal stability (T_m decreases to 43.31 ± 0.05 °C for 3 equiv), the addition of 4, 5 or 10 equiv of metal ion have a milder impact on the T_m value (Fig. 2c and Table S2); in fact, the T_m at 10 equiv of Hg(II) recovers to 59.05 ± 0.02 °C. The biphasic behavior of the thermal stability of HγC crystallin as a function of metal:protein ratio (red trace in Fig. 2g) is inversely proportional to the biphasic behavior of the extent of aggregation observed at the end point of the turbidity assay at each metal concentration (blue trace in Fig. 2g). In fact, the two traces correlate well, indicating that at 3 equiv of Hg(II) ions there is a maximum of Hg-induced aggregation that is likely due to a minimum in thermal stability at such metal:protein ratio. This correlation reveals that very distinct Hg–protein interactions must be occurring at low (< 3 equiv of Hg) and high (> 3 equiv) metal:protein ratios, leading to the formation of different metal–protein complexes with competing effects on thermal stability and extent of Hg-induced aggregation of HγC crystallin.

CD spectroscopy was also used to evaluate the impact of Hg(II) ions in protein folding. Titrations of HγC and HγS crystallin with the metal ion were followed by CD at 20 °C, as shown in Fig. 2e, f, respectively. For HγS crystallin, the addition of 1–4 equiv of Hg(II) ions causes a gradual and mild decrease on the intensity of the 218 nm negative CD signal, indicating loss of β-sheet secondary structure (Fig. 2f). A trace of the remaining folded fraction is plotted against the number of equivalents of metal ion in Figure H, and it correlates well with the loss of thermal stability in the first 4 equiv of Hg(II). The loss of secondary structure also correlates well with an increase in the extent of Hg-induced aggregation of HγS crystallin, as in both cases the effects reach a plateau at 4 equiv of metal ion. Overall, these results indicate that the key Hg–protein interactions that lead to loss of protein folding, decreased thermal stability and metal-induced aggregation of HγS crystallin must occur upon addition of the first 4 equiv of metal ions.

On the other hand, for HγC crystallin, while the addition of the first 3 equiv of Hg(II) causes a drastic decrease in the intensity of the 218 nm negative CD signal, indicating the loss of ~ 40% of the secondary structure, the addition of more equivalents have little further effect (Fig. 2e and green trace in Fig. 2g). It should be noted that the drastic loss of secondary structure caused by the first equivalents of Hg(II) ions correlate well with a loss of thermal stability and an increased Hg-induced aggregation of HγC crystallin, reaching a maximum at 3 equiv (Fig. 2g). Thus, these results indicate that the metal–protein interactions that occur at low metal:protein ratios (< 3 equiv of Hg) must be associated with partial unfolding of the protein, loss of thermal stability and Hg-induced aggregation of HγC crystallin.

Differential effects of Hg(II) ions in the N- and C-terminal domains of HγC and HγS crystallins

To gain further insight into the mechanism of Hg-induced aggregation of HγC and HγS crystallins, the impact of this metal ion in the aggregation, folding and thermal stability of the separate domains of the proteins was evaluated (Figs. 3, 4). Constructs for the separate N- and C-terminal domains of each protein could be produced, yielding stable proteins that do not aggregate, even after incubation at 37 °C (black traces in Figs. 3a, b and 4a, b). However, turbidity assays show that both the N-terminal and the C-terminal domains of both crystallins are susceptible to mercury-induced aggregation. The differentials effects of Hg(II) ions on the domains are discussed below for each protein.

For HγC crystallin, the N-(Fig. 3a) and C-terminal (Fig. 3b) domains are both prone to Hg-induced aggregation, the extent of aggregation increases with the metal:protein ratio and saturates after 2 or 3 equiv of Hg(II) (blue traces in Fig. 3g, h). Interestingly, none of the domains show the biphasic behavior displayed by the full protein (Fig. 2a, g). Thermal denaturation experiments with the separate domains of HγC crystallin in the presence of 0–4 equiv of Hg(II) ions are shown in Fig. 3c, d. A $T_m = 73.02 \pm 1.44$ °C can be determined for the N-terminal domain, while the value for the C-term is $T_m = 74.14 \pm 1.81$ °C. In both cases, the addition of Hg(II) ions cause a decrease in thermal stability (Fig. 3c, d, Table S3); however, in contrast to that observed in the full protein, no biphasic behavior was observed (red traces in Fig. 3g, h). These results clearly indicate that the metal–protein interactions that lead to the biphasic behavior in Hg-induced aggregation and loss of thermal stability require both domains to be present. Finally, the impact of Hg(II) ions in the protein folding of each domain was assessed by CD spectroscopy at 20 °C. For both the N-term (Fig. 3e) and the C-term (Fig. 3f) domains, the addition of mercury causes a gradual and mild decrease on the intensity of the 218 nm negative CD signal, indicating loss of β-sheet secondary structure. However, the extent of Hg-induced protein unfolding is much larger in the N-terminal domain, for which only 50% of the protein remains folded upon addition of > 4 equiv of Hg(II) ions; as compared to the C-term domain, where 70% of the protein remains folded even after the addition of 5 equiv of metal ion (green traces in Fig. 3g, h).

Overall, there results indicate that the mechanism of Hg-induced aggregation of the separate domains of HγC crystallin involves loss of thermal stability and protein folding, although the impact on the folding is significantly larger for the N-terminal domain. However, most importantly, the interesting biphasic behavior observed for the Hg-induced

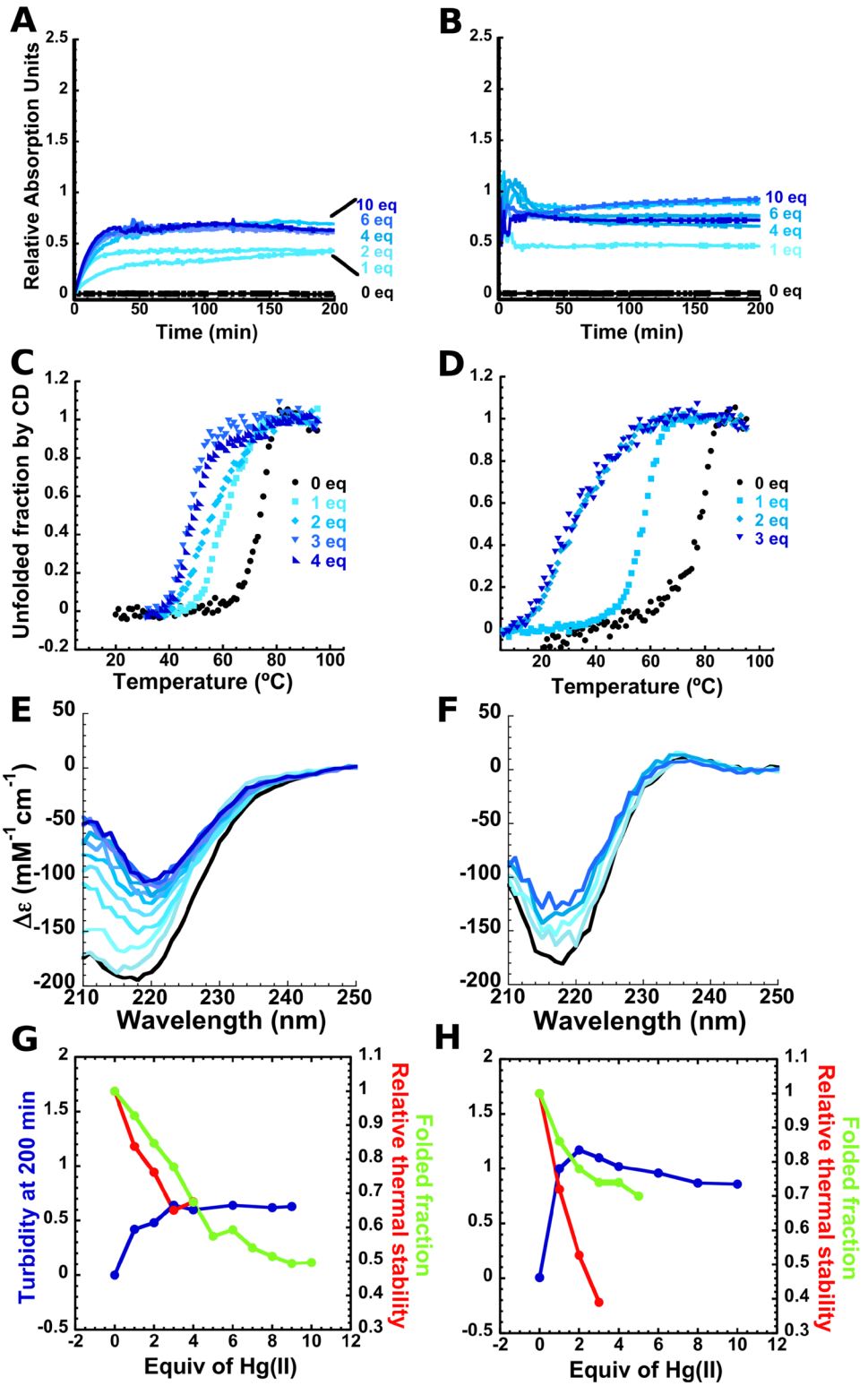

Fig. 3 Turbidity assays of the N- (**a**) and C-terminal (**b**) domains of HγC crystallin (50 μM) in the absence (black) or presence 1, 2, 4, 6, 8 and 10 equiv of Hg(II) (light to dark blue traces). All assays were performed at 37 °C, and turbidity at 400 nm was followed after the addition of Hg(II). Thermal denaturation of the N- (**c**) and C-terminal (**d**) domains of HγC crystallin (2 μM) was followed by CD in the presence of 0, 1, 2, 3 or 4 equiv of Hg(II). The fraction of unfolded protein is plotted as a function of temperature, and the associated T_m values are listed in Table S3. Titrations of the N- (**e**) and C-terminal (**f**) domains of HγC crystallin (2 μM) with 0 (black), 1, 2, 3, 4, 5, 6, 7, 8, 9 and 10 equiv of Hg(II) (light to dark blue traces), as followed by CD at 20 °C. Traces for turbidity, fraction of folded protein, and relative thermal stability, as a function of the number of equivalents of Hg(II) ions for the N- (**g**) and C-terminal (**h**) domains of HγC crystallin are also plotted

aggregation of the full protein (Fig. 2g) is abolished when the experiment is performed with the separate domains. Thus, the metal–protein interactions that occur at higher metal:protein ratios and lead to a decreased effect in aggregation must involve interactions between both domains of HγC crystallin.

On the other hand, the N-(Fig. 4a) and C-terminal (Fig. 4b) domains of HγS crystallin are also both prone

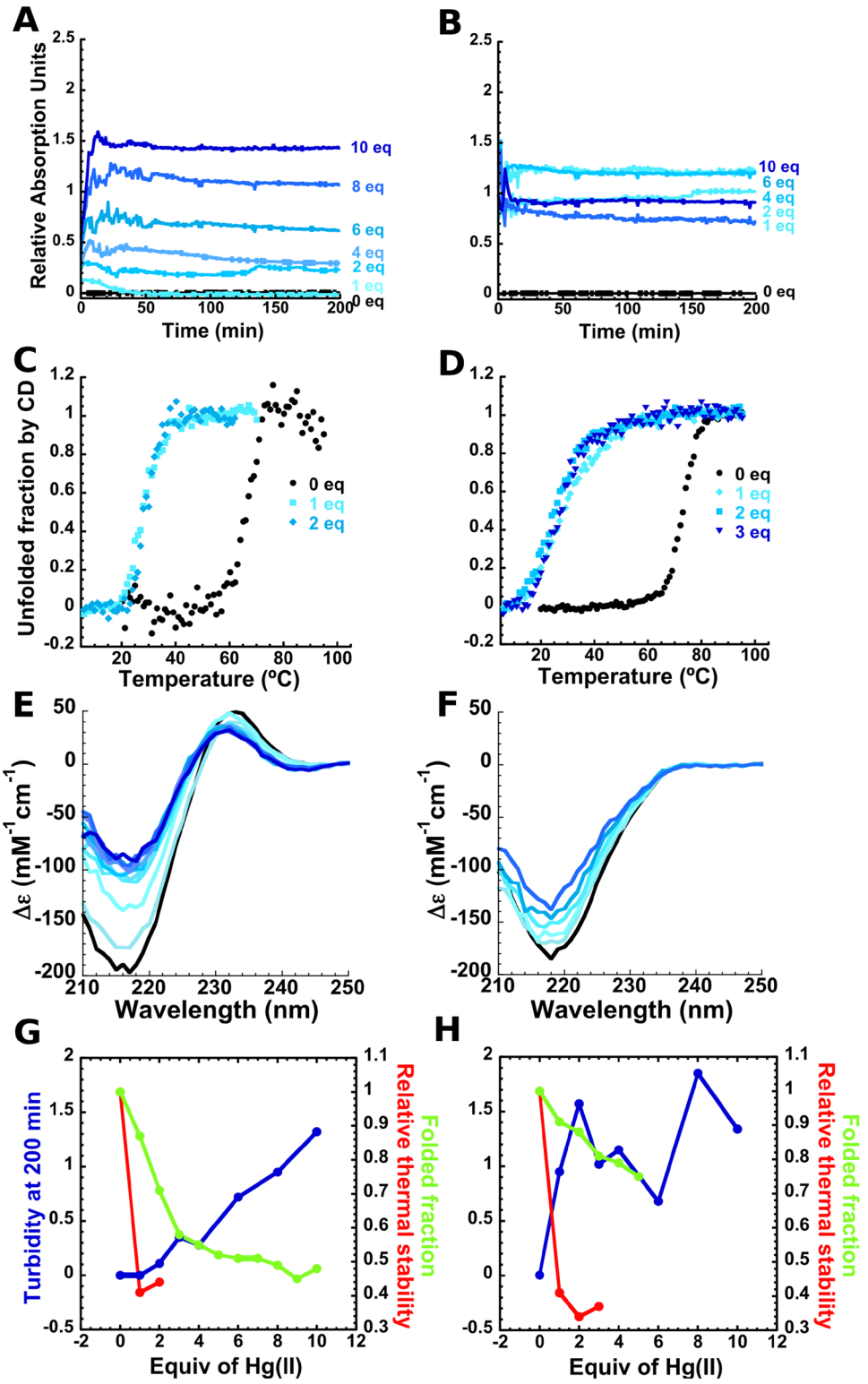

Fig. 4 Turbidity assays of the N- (**a**) and C-terminal (**b**) domains of HγS crystallin (50 μM) in the absence (black) or presence of 1, 2, 4, 6, 8 and 10 equiv of Hg(II) (light to dark blue traces). All assays were performed at 37 °C, and turbidity at 400 nm was followed after the addition of Hg(II). Thermal denaturation of the N- (**c**) and C-terminal (**d**) domains of HγS crystallin (2 μM) was followed by CD in the presence of 0, 1, 2 or 3 equiv of Hg(II). The fraction of unfolded protein is plotted as a function of temperature, and the associated T_m values are listed in Table S4. Titrations of the N- (**e**) and C-terminal (**f**) domains of HγS crystallin (2 μM) with 0 (black), 1, 2, 3, 4, 5, 6, 7, 8, 9 and 10 equiv of Hg(II) (light to dark blue traces), as followed by CD at 20 °C. Traces for turbidity, fraction of folded protein and relative thermal stability, as a function of the number of equivalents of Hg(II) ions for the N- (**g**) and C-terminal (**h**) domains of HγS crystallin are also plotted

to Hg-induced aggregation. While the extent of aggregation of the N-terminal domain increases gradually with the metal:protein ratio, the effect on the C-term domain saturates after 2 or 3 equiv of Hg(II) (blue traces in Fig. 4g, h). Thermal denaturation experiments show that the addition of Hg(II) ions cause a drastic decrease in thermal stability for both domains (Fig. 4c, d, Table S4). Although a lower T_m value (65.12 ± 1.56 °C) can be determined for the

N-terminal domain, as compared to that of the C-terminal domain ($T_m = 73.22 \pm 0.5$ °C), the addition of the first equiv of Hg(II) yields a drastic decrease in both domains, down to 27.08 ± 0.79 and 30.02 ± 1.96 °C, respectively. Finally, the addition of mercury also causes a gradual and mild decrease in the intensity of the 218 nm negative CD signal at 20 °C, indicating loss of β-sheet secondary structure for both, the N-term (Fig. 4e) and the C-term (Fig. 4f) domains. Similarly to the case of H**γ**C crystallin, the extent of Hg-induced protein unfolding is much larger in the N-terminal domain of H**γ**S crystallin, for which only 50% of the protein remains folded upon addition of > 3 equiv of Hg(II) ions, as compared to the C-term domain, where 70% of the protein remains folded even after the addition of 5 equiv of metal ion (green traces in Fig. 4g, h). Overall, these results indicate that the mechanism of Hg-induced aggregation of the separate domains of H**γ**S crystallin involves loss of thermal stability and protein folding, although the impact on the folding is significantly larger for the N-terminal domain.

Hg(II) ions induce formation of disulfide-bridged dimers involving the N-terminal domains

SDS-PAGE analysis of the Hg-induced aggregates of H**γ**C and H**γ**S crystallins was performed; in both cases, the denatured aggregates led to a very intense band at ~ 20 kDa, which corresponds to the molecular weight of the monomeric proteins (Fig. 5a, d, respectively). These results indicate that the metal-induced aggregates are composed of mostly monomeric units of γ-crystallin. However, a second band at ~ 37 kDa was also detected at higher Hg:protein ratios (red arrows in Fig. 5a, d), which might correspond to a dimeric species. The intensity of the band at ~ 37 kDa is very faint for the H**γ**C aggregates (Fig. 5a), while it is significantly more intense for H**γ**S crystallin and it appears at Hg:protein ratios higher than 3 equiv (Fig. 5d). It is important to note that this band at ~ 37 kDa completely disappears when the SDS-PAGE analysis of the Hg-induced aggregates is performed in the presence of reducing agents, such as β-mercaptoethanol (data not shown), suggesting that these dimeric species may be disulfide bridged.

The Hg-induced aggregates of the separate domains of both proteins were also analyzed by SDS-PAGE (Fig. 5 b, c, e, f). In all cases, a very intense band at ~ 10 kDa is observed, which corresponds to the molecular weight of the monomeric domains. However, a second species is also observed between 15 and 20 kDa, only in the Hg-induced aggregates of the N-terminal domains of H**γ**C (Fig. 5b) and H**γ**S (Fig. 5e) crystallins. These bands might correspond to disulfide-bridged dimeric species for each domain, since they are no longer observed when the SDS-PAGE analysis is performed in the presence of β-mercaptoethanol (data not shown). Similarly to the case of the full proteins, the presence of disulfide-bridged species is much more evident for the N-terminal domain of H**γ**S at Hg:protein ratios higher than 2 equiv (Fig. 5e), as compared to H**γ**C (Fig. 5b). It is important to note that SDS-PAGE analysis of aggregates formed with the C-terminal domains does not display any disulfide-bridged species (Fig. 5c, f).

Overall, these results suggest that the mechanism of Hg-induced aggregation of H**γ**C and H**γ**S crystallins may involve formation of disulfide-bridged dimeric species, where amino acid residues at the N-terminal domains of these proteins may be engaged.

Putative Hg(II) binding sites and mechanisms of Hg-induced aggregation of HγC and HγS crystallins

Hg(II) ions have a preference to coordinate soft ligands, such as Cys residues, usually in a bi-coordinate fashion. Indeed, preliminary electronic absorption data of titrations of H**γ**C and H**γ**S crystallins with Hg(II) ions display ligand to metal charge transfer (LMCT) bands at ~ 297 nm (~ 33,670 cm^{-1}) and ~ 235 nm (~ 42,550 cm^{-1}), which are indicative of Cys sulfur-based coordination to Hg ions (Figure S3) [45]. A more detailed spectroscopic characterization of the interactions of Hg(II) ions with H**γ**C and H**γ**S crystallins would be needed to elucidate the coordination modes involved; however, it is clear that Cys sulfur-based ligands are involved in Hg(II) coordination.

γ-crystallins contain several Cys residues (Scheme 1 and Fig. 6). H**γ**D crystallin contains a total of 6 Cys residues. Two of them, Cys 109 and 111, are located in the C-terminal domain, and are arranged in a way that they could accommodate a linear bi-coordinate geometry. Since this pair of Cys residues is absent in H**γ**C and H**γ**S crystallins, where only Cys109 is conserved, we speculate that the Cys109/Cys111 pair might be a binding site for Hg(II) ions in H**γ**D crystallin that does not cause aggregation. In contrast, for H**γ**C and H**γ**S crystallins, their C-terminal domains have a second Cys residue that is solvent exposed (Cys153 and Cys130, respectively), which could engage in metal-bridging mechanisms. Indeed, our results indicate that the mechanism of Hg-induced aggregation of the C-terminal domains does not involve disulfide-bridged species and it has a smaller contribution of partial unfolding events (as compared to the N-terminals); thus, it is likely that the dominant mechanism at the C-terminal domains involves the formation of metal-bridged species (Fig. 7).

On the other hand, the N-terminal domains of **γ**-crystallins generally contain a higher number of Cys

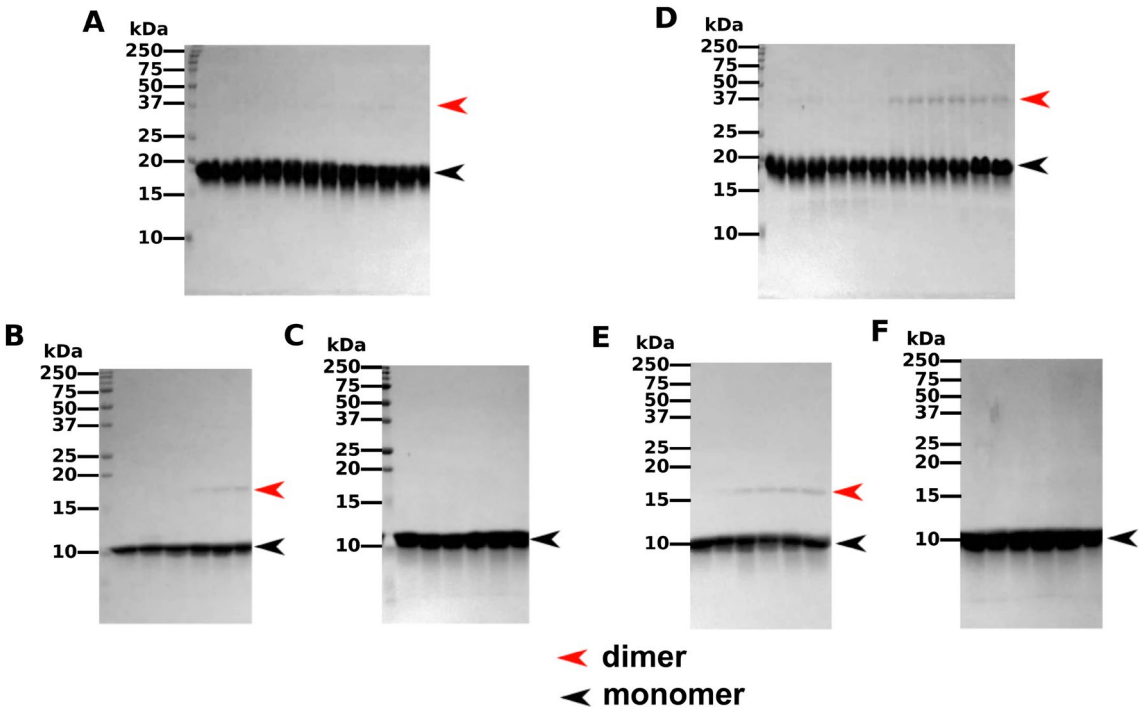

Fig. 5 SDS-PAGE analysis of the metal-induced aggregates of wt (**a**), N- (**b**), and C-(**c**) terminal domains of HγC crystallin, and wt (**d**), N- (**e**), C-terminal (**f**) domains of HγS crystallin. Aggregates of wt HγC and HγS crystallins were obtained at the end of turbidity assays with increasing amounts of Hg(II) (0, 1, 1.5, 2, 2.5, 3, 3.5, 4, 6, 8 and 10 equiv). Aggregates of N- (**b** and **e**) and C-terminal (**c** and **f**) domains of HγC and HγS crystallin were obtained at the end of turbidity assays with 2, 4, 6, 8 and 10 equiv of Hg(II). All aggregates were analyzed by SDS-PAGE after denaturation by boiling samples in SDS solutions without β-mercaptoethanol

residues, as compared to their C-terminal domains; and these residues are present in a localized region of the protein (Fig. 6). While the N-terminal domain of H**γ**D crystallin only contains 4 Cys residues, and two of them are in an arrangement that could accommodate a bi-coordinate Hg(II); H**γ**C and H**γ**S crystallins have five Cys residues, and most of them are clustered in a solvent-exposed region of the N-terminal domain. In particular, it is interesting to note that Cys22 is conserved in H**γ**C and H**γ**S crystallins, while that residue is a His22 in H**γ**D crystallin, which is not susceptible to Hg-induced aggregation; thus, it is tempting to propose that having a Cys residue at position 22 may be key for the Hg-induced aggregation of H**γ**C and H**γ**S crystallins, and perhaps the formation of disulfide-bridged species at the N-terminal region. H**γ**C and H**γ**S crystallin aggregates only contain monomeric or disulfide-bridged dimers, while no evidence for covalently linked higher molecular weight species was observed. This observation, along with the fact that only the N-terminal domains of these proteins can yield disulfide-bridged species, strongly suggests that the disulfide bridge in the dimeric species must be formed between N-terminal Cys residues of two monomers, leading to a closed

```
HγD Homo sapiens 1-173   1 -----GKITLYEDRGFQGRHYECSSDHPNLQPYLSRCNSARVDSGCWMLYEQPNYSGLQY 55
HγC Homo sapiens 1-173   1 -----GKITFYEDRAFQGRSYETTTDCPNLQPYFSRCNSIRVESGCWMLYERPNYQGQQY 55
HγS Homo sapiens 1-178   1 GSKTGTKITFYEDKNFQGRRYDCDCDCADFHTYLSRCNSIKVEGGTWAVYERPNFAGYMY 60

HγD Homo sapiens 1-173  56 FLRRGDYADHQQWMGLSDSVRSCR--LIPHSGSHRIRLYEREDYRGQMIEFTEDCSCLQD 113
HγC Homo sapiens 1-173  56 LLRRGEYPDYQQWMGLSDSIRSCC--LIPQTVSHRLRLYEREDHKGLMMELSEDCPSIQD 113
HγS Homo sapiens 1-178  61 ILPQGEYPEYQRWMGLNDRLSSCRAVHLPSGGQYKIQIFEKGDFSGQMYETTEDCPSIME 120

HγD Homo sapiens 1-173 114 RFRFNEIHSLNVLEGSWVLYELSNYRGRQYLLMPGDYRRYQDWGATNARVGSLRRVIDFS 173
HγC Homo sapiens 1-173 114 RFHLSEIRSLHVLEGCWVLYELPNYRGRQYLLRPQEYRRCQDWGAMDAKAGSLRRVVDLY 173
HγS Homo sapiens 1-178 121 QFHMREIHSCKVLEGVWIFYELPNYRGRQYLLDKKEYRKPIDWGAASPAVQSFRRIVE-- 178
```

Scheme 1 Sequence alignment of HγD (PDB: 1HK0), HγC (PDB: 2NBR) and HγS (PDB: 2M3T) crystallin proteins. All cysteine residues are highlighted with red color

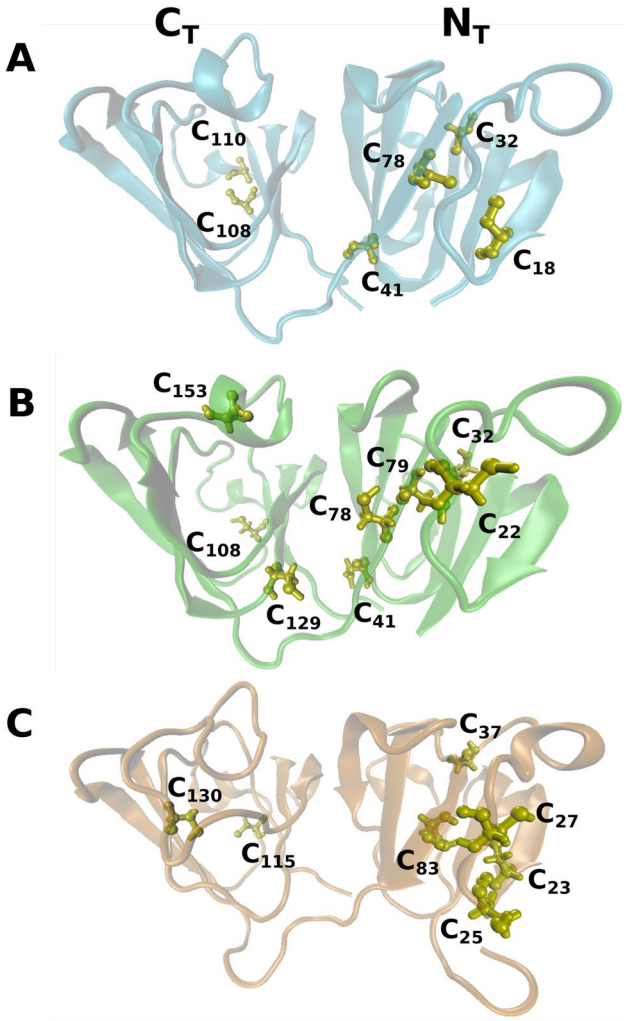

Fig. 6 Structures of HγD (**a**), HγC (**b**) and HγS (**c**) crystallins, showing the positions of all cysteine residues in each protein

dimer (Fig. 7). Further aggregation of these dimeric species likely involves metal-bridging mechanisms using Cys residues from the C-terminal domains, as discussed above.

Our results indicate that Hg-induced unfolding plays an important role in metal-induced aggregation of γ-crystallins, and this phenomenon is more pronounced at the N-terminal domain, consistent with the fact that this domain is more susceptible to loss of protein folding, as compared to the C-terminal domain [14]. Several Cys residues engaged in β-sheet secondary structural elements could be identified in the structures of H**γ**C and H**γ**S crystallins. A unique arrangement for a Cys pair, Cys78 and Cys79, contained in a β-sheet structure is found in H**γ**C crystallin, and it might be the structural motif responsible for the drastic Hg-induced unfolding observed in this protein upon addition of the first 3 equiv of metal ion. Interestingly, these two Cys residues were found to form a disulfide bond in a lens proteomic study [46]. Cys 41 and Cys129 constitute another unique Cys pair in H**γ**C crystallin (Fig. 6), which is located at the interface between the N- and C-terminal domains. It is likely that the Cys41/Cys129 pair is responsible for the unique biphasic behavior observed in Hg-induced aggregation of H**γ**C crystallin, as this protein is the only **γ**-crystallin with such a unique pair. Bi-coordinate Hg(II) coordination at this site might strengthen the inter-domain interaction, leading to the stabilizing effects observed for H**γ**C crystallin at metal:protein ratios higher than 3 equivalents (Fig. 7). This proposal is consistent with the observation that the biphasic behavior was abolished when using the separate domains.

Conclusions

In this study, we have evaluated the effect of heavy metal ions in the protein stability and aggregation of three of the more abundant **γ**-crystallin proteins in the human lens: H**γ**D, H**γ**C and H**γ**S crystallins. Our study reveals that Hg(II) ions specifically induce the non-amyloid aggregation of H**γ**C and H**γ**S crystallins, while H**γ**D crystallin is not sensitive to this metal ion. Mercury-induced aggregation of H**γ**C and H**γ**S crystallins occurs through diverse mechanisms including: metal-induced loss of stability and partial unfolding of the proteins, formation of disulfide-bridged dimeric species, and potentially through metal-bridging pathways (Fig. 7). The interaction of Hg(II) with these **γ**-crystallins likely involves Cys residues, especially at the Cys-rich N-terminal domains of H**γ**C and H**γ**S, where the metal ion causes partial unfolding of the protein. Further spectroscopic and site-directed mutagenesis studies must shed light into the nature of these mercury–crystallin interactions and their role in the mechanism of metal-induced protein aggregation. While Hg ions are not normally present in a healthy human lens, environmental exposure to this metal is a concern; and since crystallins in the core of the lens are not replaced, a one-time exposure would be enough to damage lens proteins. Thus, this study points to a potential role of this xenobiotic metal ion in the development of cataract, underscoring the bioinorganic facet of this disease.

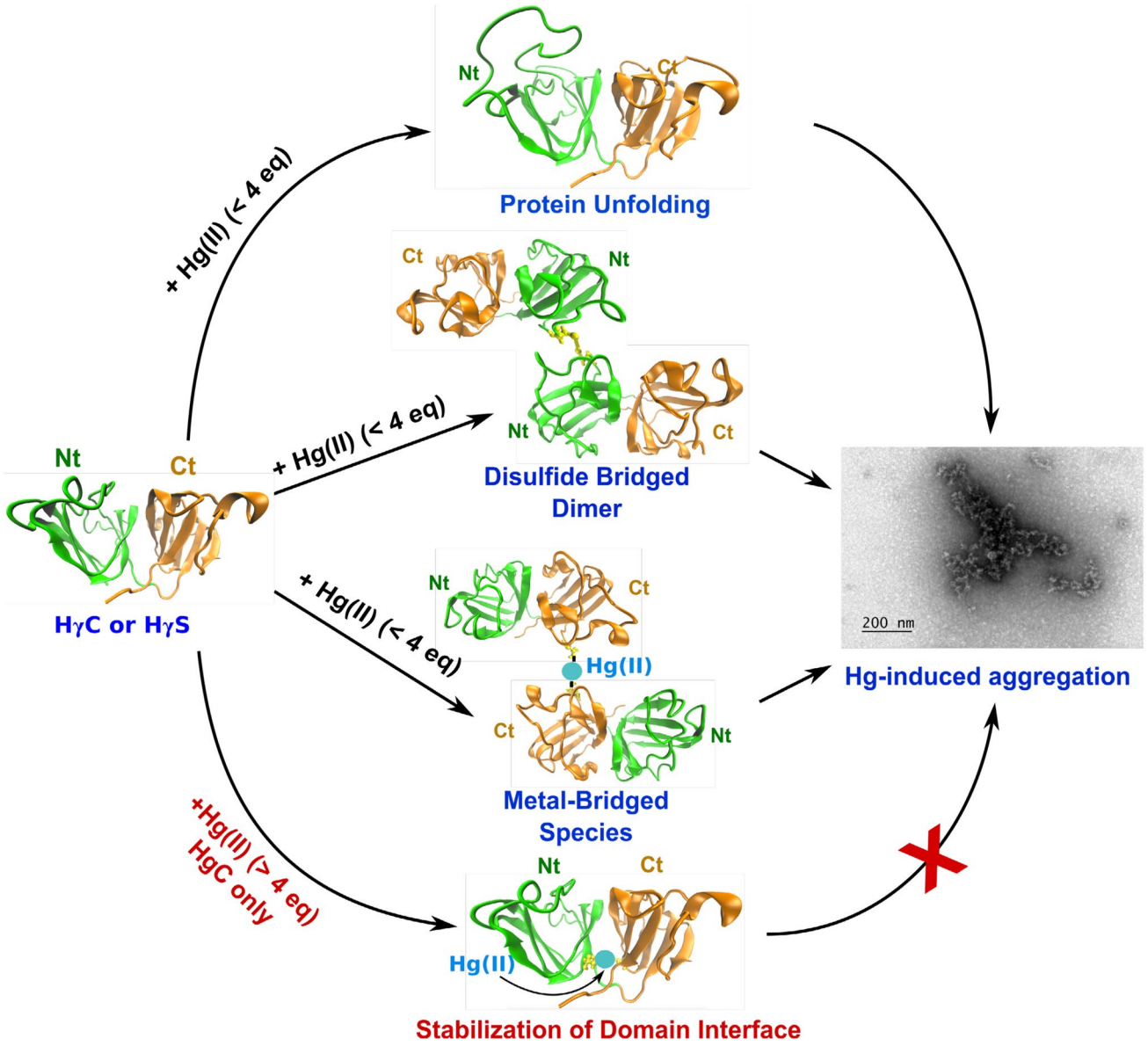

Fig. 7 Proposed mechanisms for Hg(II)-induced aggregation of HγC and HγS crystallins. At low (<4) equiv of metal ion, in both cases, three mechanisms were identified: (1) loss of protein folding, predominantly at the N-terminal domain; (2) formation of disulfide-bridged dimers involving Cys residues from the N-terminal domain; and (3) formation of metal-bridged species, likely involving Cys residues from the C-terminal domain. For HγC crystallin, at high (>4 equiv) metal:protein ratios, interaction of Hg(II) with Cys residues in the domain interface stabilizes the protein and reduces metal-induced aggregation

Acknowledgements This research has been supported by the National Council for Science and Technology in Mexico (CONACYT Grant # 221134 to L.Q. and fellowships to J.A.D.C.), MIT-Seed Funds, NIH EY015834 Grant to J.A.K., and Fulbright-García Robles fellowship and Cátedra Marcos Moshinsky to L.Q. The authors would like to thank the technical assistance of Cammeron Haase-Pettingell (at MIT) and Lourdes Rojas at the Unit of Microscopy (Cinvestav).

References

1. WHO. (2015) Visual impairment and blindness. 2015. http://www.Who.Int/mediacentre/factsheets/fs282/en/. Cited January 18, 2017
2. Moreau KL, King JA (2012) Trends Mol Med 18:273–282
3. Serebryany E, King JA (2014) Prog Biophys Mol Biol 115:32–41
4. Deloitte Access Economics (2014) The economic cost and burden of eye diseases and preventable blindness in Mexico. https://www2.deloitte.com/content/dam/Deloitte/au/Documents/Economics/deloitte-au-economics-cost-eye-diseases-280314.pdf. Accessed 7 July 2017
5. Graw J (2009) Exp Eye Res 88:173–189

6. Hains PG, Truscott RJW (2010) Invest Ophthalmol Vis Sci 51:3107–3114
7. Lampi K, Wilmarth PA, Murray MR, David LL (2014) Prog Biophys Mol Biol 115:21–31
8. Takata T, Oxford JT, Demeler B, Lampi K (2008) Protein Sci 17:1565–1575
9. Takata T, Murakami K, Toyama A, Fujii N (2018) Biochim Biophys Acta 1866:767–774
10. Haslbeck MPJ, Buchner J, Weinkauf S (2016) Biochim Biophys Acta 1860:149–166
11. Vendra VKI, Chandani S, Muniyandi A, Balasubramanian D (2016) Biochim Biophys Acta 1860:333–343
12. Acosta-Sampson L, King J (2010) J Mol Biol 401:134–152
13. Wride MA (2011) Philos Trans R Soc B-Biol Sci 366:1219–1233
14. Kosinski-Collins MS, King J (2003) Protein Sci 12:480–490
15. Serebryany E, King JA (2015) J Biol Chem 290:11491–11503
16. Serebryany E, Woodard JC, Adkar BV, Shabab M, King JA, Shakhnovich EI (2016) J Biol Chem 291:19172–19183
17. Serebryany E, Takata T, Erickson E, Schafheimer N, Wang Y, King JA (2016) Protein Sci 25:1115–1128
18. Khago D, Wong EK, Kingsley CN, Freites JA, Tobias DJ, Martin RW (2016) Biochim Biophys Acta 1860:325–332
19. Roskamp KW, Montelongo DM, Anorma CD, Bandak DN, Chua JA, Malecha KT, Martin RW (2017) Invest Ophthalmol Vis Sci 58:2397–2405
20. Boatz JC, Whitley MJ, Li M, Gronenborn AM, van der Wel PCA (2017) Nat Commun 8:15137
21. Donald H (1962) The diseases of occupations. Little, Brown and Co, Boston
22. Dawczynski J, Blum M, Winnefeld K, Strobel J (2002) Biol Trace Elem Res 90:15–23
23. Srivastava VK, Varshney N, Pandey DC (1992) Acta Ophthalmol 70:839–841
24. Cekic O (1998) Br J Ophthalmol 82:186–188
25. Langford-Smith A, Tilakaratna V, Lythgoe PR, Clark SJ, Bishop PN, Day AJ (2016) PLoS One 11:e0147576
26. Chang JR, Koo E, Agron E, Hallak J, Clemons T, Azar D, Sperduto RD, Ferris FL, Chew EY (2011) Ophthalmology 118:2113–2119
27. Ye J, He J, Wang C, Wu H, Shi X, Zhang H, Xie J, Lee SY (2012) Invest Ophthalmol Vis Sci 53:3885–3895
28. Saffari A, Daher N, Ruprecht A, De Marco C, Pozzi P, Boffi R, Hamad SH, Shafer MM, Schauer JJ, Westerdahl D, Sioutas C (2014) Environ Sci Process Impacts 16:2259–2267
29. Lemire M, Fillion M, Frenette B, Mayer A, Philibert A, Sousa Passos CJ, Davee Guimaraes JR, Barbosa F, Mergler D (2010) Environ Health Perspect 118:1584–1589
30. https://www.documentcloud.org/documents/2771769-Memo-From-Janet-McCabe-on-Art-Glass-Manf.html#document/p2/a284265. Accessed 1 Aug 2018
31. Garza-Lombo C, Posadas Y, Quintanar L, Gonsebatt ME, Franco R (2018) Antioxid Redox Signal 28:1669–1703
32. Ahmad MF, Singh D, Taiyab A, Ramakrishna T, Raman B, Rao CM (2008) J Mol Biol 382:812–824
33. Biswas A, Das KP (2008) Biochemistry 47:804–816
34. Laganowsky A, Benesch JLP, Landau M, Ding L, Sawaya MR, Cascio D, Huang Q, Robinson CV, Horwitz J, Eisenberg D (2010) Protein Sci 19:1031–1043
35. Mainz A, Bardiaux B, Kuppler F, Multhaup G, Felli IC, Pierattelli R, Reif B (2012) J Biol Chem 287:1128–1138
36. Quintanar L, Dominguez-Calva JA, Serebryany E, Rivillas-Acevedo L, Haase-Pettingell C, Amero C, King JA (2016) ACS Chem Biol 11:263–272
37. Robinson NE, Lampi KJ, Speir JP, Kruppa G, Easterling M, Robinson AB (2006) Mol Vis 12:704–711
38. Wang YPS, Trojanowski T, Knee K, Goulet D, Mukerji I, King J (2010) Invest Ophthalmol Vis Sci 51:672–678
39. Pande APJ, Asherie N, Lomakin A, Ogun O, King J, Benedek GB (2001) PNAS 98:6116–6120
40. Pande A, Pande J, Asherie N, Lomakin A, Ogun O, King JA, Lubsen NH, Walton D, Benedek GB (2000) PNAS 97:1993–1998
41. Fu L, Liang JJN (2002) FEBS Lett 513:213–216
42. Mills IA, Flaugh SL, Kosinski-Collins MS, King JA (2007) Protein Sci 16:2427–2444
43. Sun TX, Das BK, Liang JJ (1997) J Biol Chem 272:6220–6225
44. Ma Z, Piszczek G, Wingfield PT, Sergeev YV, Hejtmancik JF (2009) Biochemistry 48:7334–7341
45. Luczkowski M, Stachura M, Schirf V, Demeler B, Hemmingsen L, Pecoraro VL (2008) Inorg Chem 47:10875–10888
46. Hanson SR, Smith DL, Smith JB (1998) Exp Eye Res 67:301–312

Affiliations

J. A. Domínguez-Calva[1] · M. L. Pérez-Vázquez[1] · E. Serebryany[2] · J. A. King[2] · L. Quintanar[1]

✉ L. Quintanar
lilianaq@cinvestav.mx

[1] Departamento de Química, Centro de Investigación y de Estudios Avanzados (Cinvestav), Mexico City, Mexico

[2] Department of Biology, Massachusetts Institute of Technology, Cambridge, MA, USA